AIAA JOURNAL
Vol. 34, No. 7, July 1996

Solution for Spin-Up from Rest of Liquid with a Free Surface

Kwan Yeop Kim* and Jae Min Hyun†
Korea Advanced Institute of Science and Technology, Taejon 305-701, Republic of Korea

The problem of spin-up from rest of a liquid in a partially filled circular cylinder is considered. The Ekman number of the system, $E = \nu/\Omega R^2$, is much smaller than unity. Numerical solutions to the governing Navier–Stokes equations have been secured. The numerical results provide descriptions of the evolving free surface shape, as well as the time-dependent three-component (u, v, w) velocity field. Particular attention is given to the task of verifying the capabilities of the earlier analytical models. Numerical results for four prototypical flow configurations are examined. For all four cases, close agreement is noted in the free surface contour and azimuthal velocity field between the present numerical results and the predictions of the analytical model. Utilizing the numerical data, time-dependent meridional flowfields are depicted. These are consistent with the fundamental notions embedded in the analytical model. The present numerical study is supportive of the basic contentions of the model.

Nomenclature

Ar	= aspect ratio of the container, H/R
E	= Ekman number, $\nu/\Omega R^2$
Fr	= Froude number, $\Omega^2 R^2/(gH)$
g	= axial acceleration
H	= dimensional height of the container
h	= dimensional height of interface
L	= initial interface level before spin-up
p	= pseudopressure
R	= dimensional radius of the container
r_{TI}	= intersecting radius on the top endwall disk
r_{BI}	= intersecting radius on the bottom endwall disk
t	= dimensionless time
(u, v, w)	= velocity components corresponding to (r, θ, z)
(r, θ, z)	= radial, azimuthal, and vertical axes in cylindrical coordinate system
$\Delta\Omega$	= rotational rate change of the container, rad/s
ε	= Rossby number, $\Delta\Omega/\Omega$
ν	= kinematic viscosity of fluid
τ	= Ekman time scale, $E^{-1/2}\Omega^{-1}$
ψ	= meridional stream function
Ω	= rotational rate of the container, rad/s

Subscripts

f	= final state
i	= initial state
r, z	= derivative in radial and axial direction

I. Introduction

TRANSIENT motions of a viscous fluid in response to a change in rotation rate of the container from Ω_i to Ω_f are termed spin-up. To understand the intrinsic dynamics of the flow, geometrically simple axisymmetric cylindrical containers are usually selected for a fundamental analysis. For most technological applications, the representative Ekman number of the system is small, $E \equiv \nu/\Omega R^2 \ll 1$, in which ν denotes the fluid kinematic viscosity, Ω the characteristic rotation rate of the container, and R the characteristic dimension of the container. Studies of spin-up have occupied centerstage of classical study of unsteady rotating fluid dynamics.

Received Dec. 23, 1994; revision received Aug. 21, 1995; accepted for publication Aug. 23, 1995.

*Student, Department of Mechanical Engineering, 373-1 Kusong-dong Yusungku.

†Professor, Department of Mechanical Engineering, 373-1 Kusong-dong Yusungku.

The pioneering treatise of Greenspan and Howard[1] dealt with situations when the initial state was in a pre-existing rigid-body rotation at Ω_i in a circular cylinder. They further confined their attention to linearized problems, in which the step change in rotation rate was small, i.e., $\Delta\Omega[\equiv\Omega_f - \Omega_i] \ll \Omega_f$. It was succinctly shown that the transient process in the bulk of the container interior is accomplished by radial advection of angular momentum that is driven essentially by the Ekman layer suction mechanism. Accordingly, the global adjustment is substantially attained over the spin-up time scale $E^{-1/2}\Omega_f^{-1}$, rather than the much longer diffusive time scale $E^{-1}\Omega_f^{-1}$.

The extension of the preceding theoretical contention to strongly nonlinear flow in a cylinder, starting from the initial state of rest ($\Omega_i \equiv 0$, $\Delta\Omega = \Omega_f$), was carried out by Wedemeyer.[2] Several heuristic arguments and physical insights were incorporated in the construction of the analytical model. The crux of this model is that the interior core region is divided into a nonrotating zone and a rotating zone that are separated by a radially propagating cylindrical velocity shear front. The qualitative correctness of this model has since been established by a number of numerical and experimental investigations (e.g., Refs. 3–8).

The aforesaid classical spin-up models are concerned with the cases when the fluid completely fills the closed container. As a variation of the basic configuration, the problem of spin-up from rest of a liquid with a free surface has been studied for some time. The flow properties are of interest from the standpoint of fundamental rotating fluid dynamics research. Also, in practical engineering applications, there are situations in which the liquid fills only a part of the rotating vessel. Knowledge of the transient behavior of a partially filled fluid in a rotating container is useful for the design and operation of chemical mixers, fluid machinery, centrifuges, etc.

Goller and Ranov[9] proposed an approximate analytical model, principally based on Wedemeyer's formalism[2] to depict the free surface profile during spin-up from rest. Several plausibility arguments, enriched by physical observations, were built into the model. The predictions of this model for the evolving free surface shape were shown to be consistent with laboratory measurements. Because of the inherent limitations of the original Wedemeyer model, however, Gollar and Ranov[9] gave no descriptions of the details of flow evolution, in particular, the meridional flowfield.

Further refinements of the model were implemented by Homicz and Gerber[10,11] (H–G) extending the methodologies of the Goller and Ranov model. A number of simplifying assumptions were invoked in the course of the model construction. These efforts led to straightforward schemes to calculate the gross characteristics in the interior core and the resulting deformation of the free surface. The reliability of this model was tested by checking the analytical predictions against the laboratory measurements of transient free

surface contour by Choi et al.[12,13] These comparisons demonstrated satisfactory consistency between the two sets of data. As noted by Homicz and Gerber as well as by Choi et al.,[12,13] however, experimental data on comprehensive flow details in the entire cylinder interior have not been available in the published literature. It should be pointed out that in spin-up flows with $E \ll 1$ the meridional velocities are $\mathcal{O}(E^{1/2})$ of the primary azimuthal velocity. Consequently, direct experimental measurements of the meridional flows are formidable undertakings, although the meridional flows are essential ingredients in the evolution of a global flowfield. In view of this practical difficulty, one alternative is to seek numerical solutions to the governing equations, and the present paper reports the results of such numerical endeavors. The numerical results of time-dependent azimuthal velocity will be compared with the predictions based on the prior analytical model. These exercises will give credence to the validity of the present numerical results. Utilizing these verified numerical solutions, features of transient meridional circulations will be explored.

One mission of this work is to make a critical assessment of the capabilities of the Gollar and Ranov[9] model and of the H–G[10,11] model by utilizing the numerical solutions of the unapproximated governing equations. Particular emphasis is placed on the model predictions of free surface displacement, including the cases when the free surface intersects the endwall disk(s). Another purpose is to portray the principal structure of both azimuthal and meridional velocities throughout the entire flow domain. Plots describing the flow evolution are illustrated. These depictions were made possible by using flow data acquired by numerical simulations. In summary, the present numerical solutions are complementary to the previous H–G[10,11] analytical model, and the present results reinforce the qualitative characterizations of the flow structure that have been put forth by formulations of the prior authors.

II. Formulation

Consider a vertically mounted closed cylindrical container (radius R, height H) that is partially-filled by a liquid (density ρ, kinematic viscosity ν). At the initial state of rest, the liquid level is L. At $t = 0$, the system abruptly begins to rotate at angular frequency Ω about the central longitudinal axis z (see Fig. 1). The task is to describe the ensuing motion of liquid. As remarked by Homicz and Gerber[10,11] and Choi et al.,[12,13] the global flowfield may be classified into four different patterns, depending on the shape of the final-state free surface. Figure 2 shows these four patterns, which were previously presented by Gerber.[14] Clearly, in the final state, the free surface touches only the sidewall (stage 1), or one of the two endwall disks (stages 2a and 2b), or both of the endwall disks (stage 3).

Adopting a cylindrical frame (r, θ, z), with corresponding velocity components (u, v, w), the governing time-dependent, axisymmetric, Navier–Stokes equations in dimensionless form are

$$\frac{1}{r}\frac{\partial}{\partial r}(ru) + \frac{\partial w}{\partial z} = 0$$

$$\frac{\partial u}{\partial t} + u\frac{\partial u}{\partial r} + w\frac{\partial u}{\partial z} - \frac{v^2}{r} = -\frac{\partial p}{\partial r} + E\left(\nabla^2 u - \frac{u}{r^2}\right)$$

$$\frac{\partial v}{\partial t} + u\frac{\partial v}{\partial r} + w\frac{\partial v}{\partial z} + \frac{uv}{r} = E\left(\nabla^2 v - \frac{v}{r^2}\right) \qquad (1)$$

$$\frac{\partial w}{\partial t} + u\frac{\partial w}{\partial r} + w\frac{\partial w}{\partial z} = -\frac{\partial p}{\partial z} - \frac{1}{Ar \cdot Fr} - E(\nabla^2 w)$$

$$\nabla^2 \equiv \frac{1}{r}\frac{\partial}{\partial}\left(r\frac{\partial}{\partial r}\right) + \frac{\partial^2}{\partial z^2}$$

In Eqs. (1) nondimensionalization has been made by using R, $R\Omega$, and Ω^{-1} as reference values for length, velocity, and time, respectively. In Eqs. (1), the Froude number $Fr \equiv \Omega^2 R^2/(gH)$, the cylinder aspect ratio $Ar \equiv H/R$, the Ekman number $E \equiv \nu/R\Omega^2$, and the Reynolds number is $Re \equiv E^{-1}$.

The initial conditions at $t = 0$ are

$$u = v = w = 0 \qquad 0 \le r \le 1, \qquad 0 \le z \le L/R \qquad (2)$$

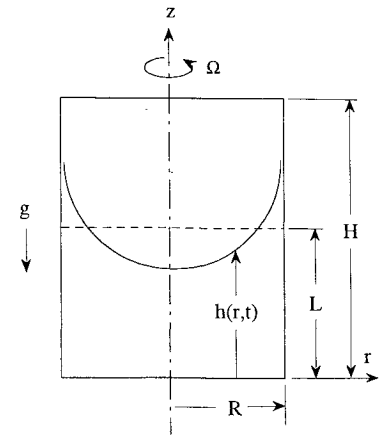

Fig. 1 Schema of flow configuration.

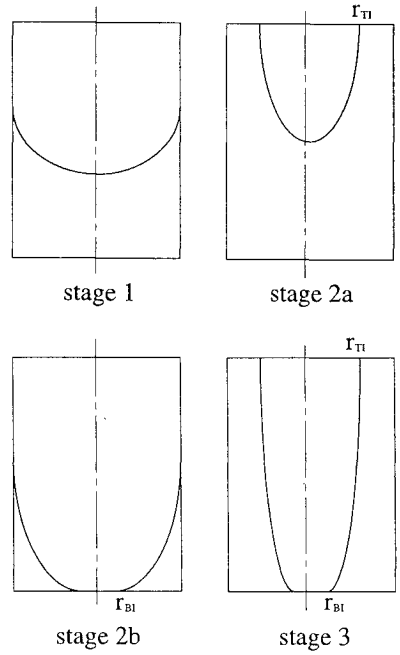

Fig. 2 Four representative final-state configurations, as described by Gerber.[14]

After the cylinder is set in rotation, the nondimensional height of the deforming free surface is denoted by $h(r, t)$. Disregarding the surface tension effect, the boundary conditions for $t>0$ may be stated as

$$u = v = 0, \qquad \frac{\partial w}{\partial r} = 0 \quad \text{at} \quad r = r_i, \qquad 0 \le z \le h(r_i, t) \qquad (3a)$$

$$u = w = 0, \qquad v = 1 \quad \text{at} \quad r = 1, \qquad 0 \le z \le h(1, t) \qquad (3b)$$

$$u = w = 0, \qquad v = r \quad \text{at} \quad \begin{cases} r \ge r_{TI}, & z = H/R \\ r > r_{BI}, & z = 0 \end{cases} \qquad (3c)$$

$$p = 0, \qquad \frac{\partial h}{\partial t} + u\frac{\partial h}{\partial r} - w = 0 \qquad \text{on} \quad z = h(r, t) \qquad (3d)$$

The symmetry condition at the central axis is enforced at $r = r_i$, a small but nonzero radius, as in Eq. (3a). This is a customary numerical practice to avoid the singularity at the axis (e.g., Ref. 15). The nonslip conditions at the solid walls are applied only at the wetted zones. Obviously, if the free surface intersects only the cylindrical sidewall ($r=1$), Eq. (3c) is applied at $z = 0$ and $0 < r \le 1$. If the free surface intersects one or both of the endwall disks [$r_{BI}(t)$ and $r_{TI}(t)$ are the intersecting radius on the bottom and top endwall disk, respectively], however, then Eq. (3c) is applicable only to the regions between these intersecting radii and the side wall, e.g., Refs. 10 and 11 (see Fig. 2).

The system of equations is subject to finite difference numerical ntegration. The grid was stretched to cluster more mesh points near he solid walls and the region of deforming free surface. The ad-'ective terms were represented by using the power law advocated)y Patankar.[16] The computation of the free surface profile was per-ormed by employing the volume-of-fluid (VOF) technique of Hirt ınd Nichols.[17] Time marching was done using the explicit scheme, ınd very small time steps were employed to be in line with the /OF technique. The projection method of Peyret and Taylor[18] was ıtilized to solve the Poisson equation for pressure; this has the ad-'antage of handling complex boundary conditions. An example of he finite difference equation and the derivation of formal accuracy)f the method can be found in Patankar.[16] The implementation of he VOF, in conjunction with the grid stretching method, is doc-ımented in detail in Hirt and Nichols.[17] For typical calculations, he grid network was (50 × 100) in the (r–z) meridional plane. ;everal grid and time-step convergence tests were performed, and he outcome of these tests was mutually consistent. The output of he present numerical procedure was checked against the existing :xperimental spin-up data for a two-layer liquid[19] as well as the aboratory measurements of free surface deformation (see Refs. 12 nd 13). These model validation efforts turned out to be affirmative, nd established the reliability and accuracy of the present numerical olution methodologies. Calculations were run on the CRAY-2S su-)ercomputer and took approximately 1 h of CPU time for each run.

III. Results and Discussion

Illustration and discussion of the numerical solutions will be cen-ered on four prototypical runs, which fall into the four characteristic onfigurations, respectively, displayed in Fig. 2.

Run 1:

$$E = 0.9 \times 10^{-4}, \qquad Fr = 1.377, \qquad L/H = 0.50$$

Run 2a:

$$E = 0.9 \times 10^{-4}, \qquad Fr = 1.377, \qquad L/H = 0.75$$

Run 2b:

$$E = 0.9 \times 10^{-4}, \qquad Fr = 1.377, \qquad L/H = 0.25$$

Run 3:

$$E = 0.9 \times 10^{-4}, \qquad Fr = 2.999, \qquad L/H = 0.50$$

For all of the experiments and numerical computations, the as-)ect ratio $H/R = 4.54$. Parallel calculations were also made to cquire the analytical model predictions of Homicz and Gerber.[10,11] t should be recalled that the analytical predictions are obtainable ıainly for the dominant azimuthal velocity $v(r, t)$ in the interior core nd for the free surface contour $h(r, t)$. In the calculation procedures f Homicz and Gerber,[10,11] a number of model constants are intro-ıced, and the recommended values of these empirical constants re suggested therein. In the present exercise, strict adherence to the tipulated H–G original model constants and computing routines vas enforced.

The time evolution of the free surface shape shown in Fig. 3a or run 1 is representative of the case when the final-state free sur-ace intersects only the cylindrical side wall (shown in Fig. 2). As isplayed in Fig. 3a, good agreement is seen between the present umerical results and the H–G model predictions. The radial pro-les of the azimuthal velocity v, along $z' [\equiv z(R/H)] = 0.25$, are hown in Fig. 3b. Overall consistency between the two sets of data s apparent.

A set of laboratory experiments was performed to provide cross omparisons with the numerical computations. The meridional lows (u, w) are orders-of-magnitude smaller than the azimuthal elocity (v). Therefore, no direct experimental measurements of ıeridional flows were attempted. Laser measurements of azimuthal elocities were carried out essentially using the same apparatus and xperimental methodologies of Choi et al.[12,13] As seen in Fig. 3, ıe numerical computations are shown to be consistent with the ıboratory data.

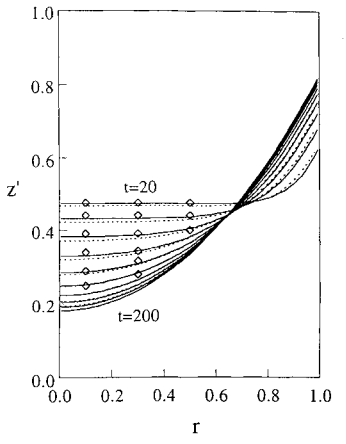

Fig. 3a Time-dependent free-surface contours for run 1: ——, present results; - - - -, prediction of H–G; and ◇, laboratory measurements. Time interval for the curves is $\Delta t = 20.0$ and ordinate $z' \equiv z(R/H)$.

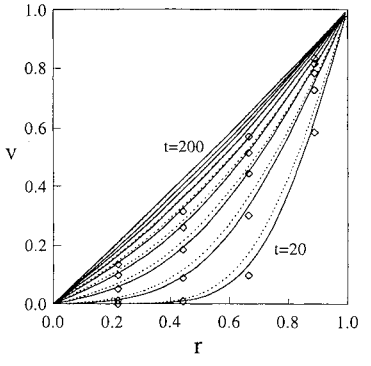

Fig. 3b Time-dependent azimuthal velocity v.

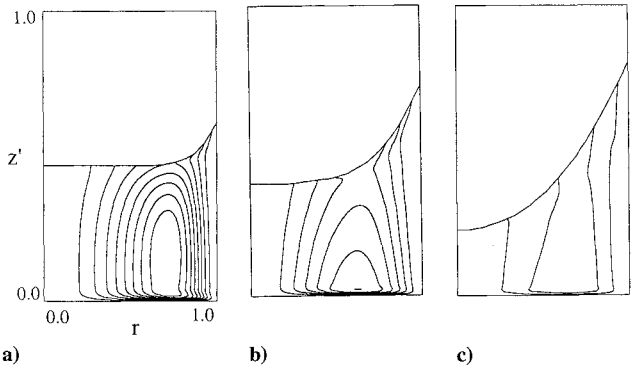

Fig. 4 Sequential plots of meridional streamfunction ψ for run 1: a) $t = 20.0$, $\psi_{max} = 5.93 \times 10^{-3}$, $\Delta\psi = 6.59 \times 10^{-4}$; b) $t = 60.0$, $\psi_{max} = 2.33 \times 10^{-3}$, $\Delta\psi = 3.88 \times 10^{-4}$; and c) $t = 140.0$, $\psi_{max} = 8.64 \times 10^{-4}$, $\Delta\psi = 2.88 \times 10^{-4}$.

Figure 4 demonstrates sequential plots showing meridional flows as well as the free surface displacement. The streamfunction ψ is defined such that $u = (1/r)(\partial\psi/\partial z)$, $w = (1/r)(\partial\psi/\partial r)$. The meridional flow induced by the bottom Ekman layer is intense at short times. As time elapses, the fluid in the interior bulk is spun up, and the meridional flow, in general, weakens accordingly. The impact of the free surface deformation on meridional circulation is noticeable, mostly in localized areas close to the free surface and in the zones where the free surface curvature is pronounced. The radially inward motion is seen to be aided by the deformation of free surface. These influences, although small in overall magnitude, are discernible in Figs. 4a and 4b in the areas adjacent to the free surface with large curvature.

Figure 5 illustrates sequential displays of azimuthal velocity. At short and moderate times, Figs. 5a and 5b clearly demonstrate the

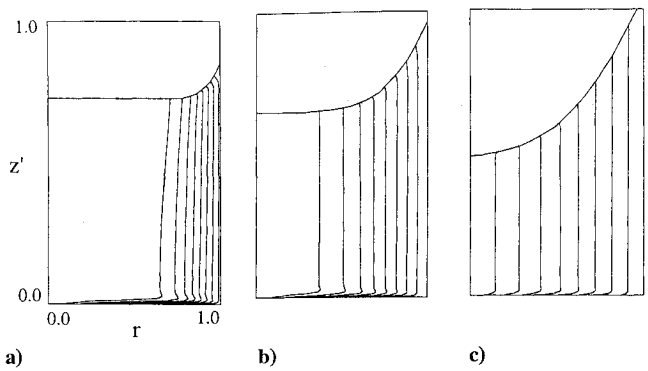

Fig. 5 Plots of the v field for run 1, $v_{max} = 1.0$ on the solid walls, and curves represent contour lines of v at equal increments $\Delta v = 0.11$: a) $t = 20.0$, b) $t = 60.0$, and c) $t = 140.0$.

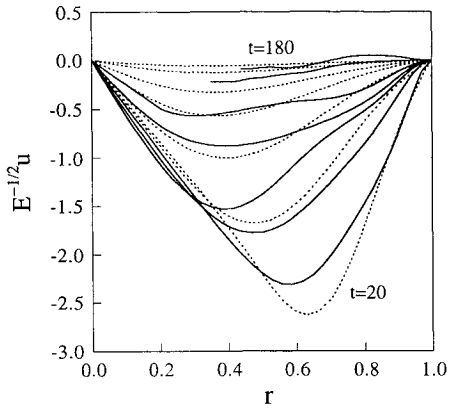

Fig. 6 Radial profiles of u along $z' = 0.25$ for run 1: ——, present results; and - - - -, predictions of H–G. Time interval for curves is $\Delta t = 20.0$.

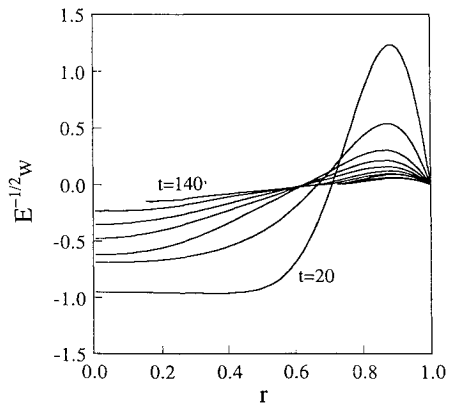

Fig. 7 Radial profiles of w along $z'=0.25$ for run 1: ——, present results; and - - - -, predictions of H–G. Time interval for curves is $\Delta t = 20.0$.

existence of a nonrotating zone and a rotating zone, which are separated by a propagating front. The axial uniformity of v in the interior is in evidence. It is noted that in small localized areas adjacent to the strongly curved free surface, the axial uniformity of v is slightly perturbed. In the bulk of the interior, however, the v field is substantially uniform in the axial direction, and the present numerical results are compatible with the observations of Choi et al.[12,13]

In an effort to scrutinize further details, illustrative plots of the radial profiles of u and w, at $z' = 0.25$ for run 1 are presented in Figs. 6 and 7. The location of $|u|_{max}$, which is directed radially inward, is seen at large radii at short times, but this location moves to smaller radii as spin up progresses. For run 1, at long time periods, say, $t \gtrsim 130.0$, the free surface deformation is such that at smaller radii the liquid height is lower than the horizontal cut $z' = 0.25$ exemplified in Figs. 5–7. As stated in the analytical model development discussion, vertical flows are predominantly downward at

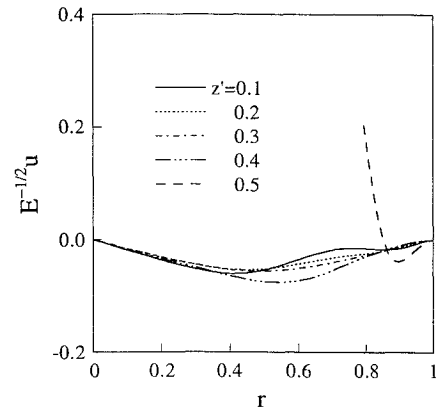

Fig. 8 Radial profiles of u for run 1, time $t = 40.0$.

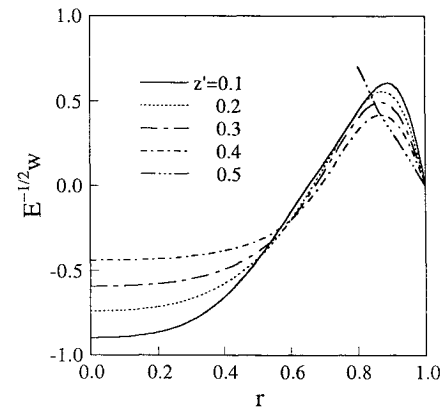

Fig. 9 Radial profiles of w for run 1, time $t = 40.0$.

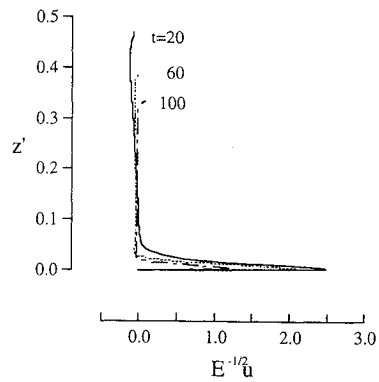

Fig. 10a Axial profiles of u for run 1 along $r = 0.5$.

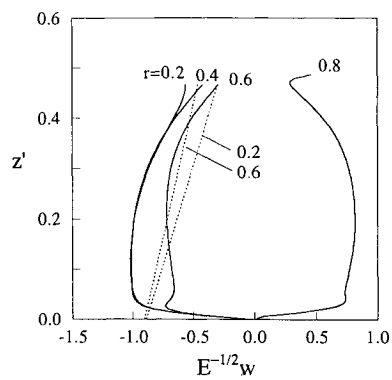

Fig. 10b Axial profiles of w for run 1 at $t = 20.0$: ——, present results; - - - -, interior-solutions of the H–G model.

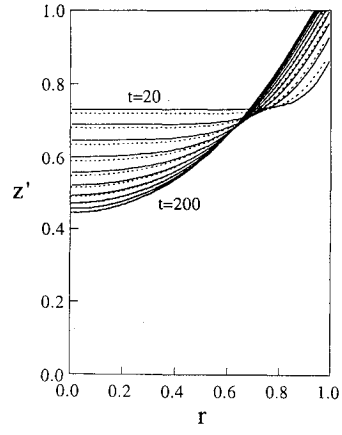

Fig. 11a Free-surface contours for run 2a: ——, present results; and - - - -, predictions of H–G. Time interval for curves is $\Delta t = 20.0$.

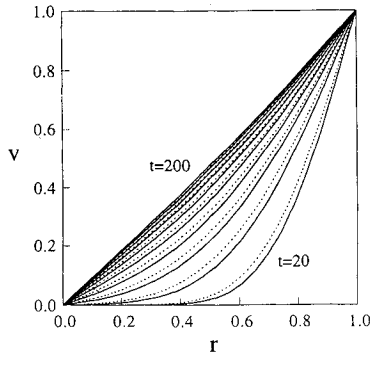

Fig. 11b Azimuthal velocity v for run 2a: ——, present results; and - - - -, predictions of H–G. Time interval for curves is $\Delta t = 20.0$.

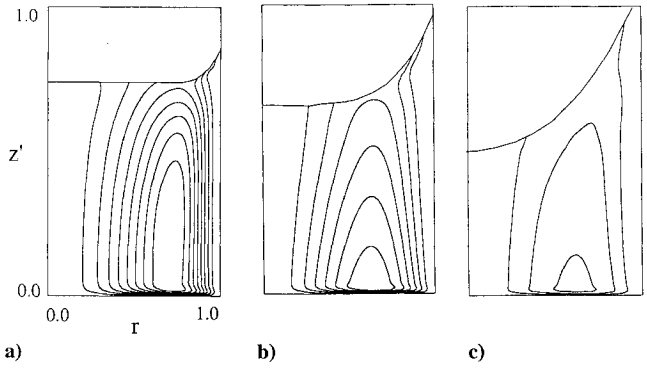

Fig. 12 Meridional streamfunction ψ for run 2a: a) $t = 20.0$, $\psi_{max} = 5.76 \times 10^{-3}$, $\Delta\psi = 6.40 \times 10^{-4}$; b) $t = 60.0$, $\psi_{max} = 2.63 \times 10^{-3}$, $\Delta\psi = 4.38 \times 10^{-4}$; and c) $t = 140.0$, $\psi_{max} = 8.05 \times 10^{-4}$, $\Delta\psi = 2.68 \times 10^{-4}$.

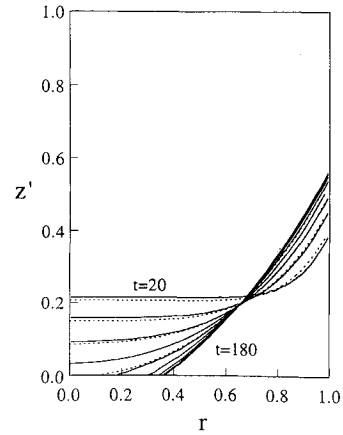

Fig. 13a Free-surface contours for run 2b: ——, present results; and - - - -, predictions of H–G. Time interval for curves is $\Delta t = 20.0$.

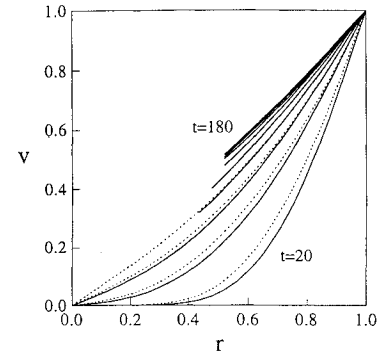

Fig. 13b Azimuthal velocity v for run 2b: ——, present results; and - - - -, predictions of H–G. Time interval for curves is $\Delta t = 20.0$.

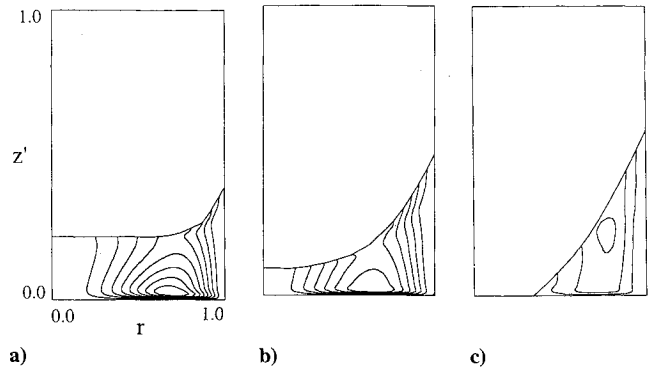

Fig. 14 Meridional streamfunction ψ for run 2b: a) $t = 20.0$, $\psi_{max} = 4.75 \times 10^{-3}$, $\Delta\psi = 5.28 \times 10^{-4}$; b) $t = 60.0$, $\psi_{max} = 1.75 \times 10^{-3}$, $\Delta\psi = 2.92 \times 10^{-4}$; and c) $t = 140.0$, $\psi_{max} = 8.18 \times 10^{-4}$, $\Delta\psi = 2.73 \times 10^{-4}$.

small and moderate radii and are driven by the Ekman pumping. The vertically upward return circuit is noticeable at large radii close to the sidewall. A close inspection of the meridional flow structure is made in Figs. 8–10. Note in Fig. 8 that the free surface has deformed considerably and that at this time instant the free surface intersects the horizontal cut $z' = 0.5$ at $r \cong 0.8$. No liquid exists for $r \lesssim 0.8$ at this vertical level ($z' = 0.5$). As demonstrated in Fig. 8, the radial velocities are mostly radially inward (u negative) in much of the liquid interior. At vertical level $z' = 0.5$, however, due to the pronounced influence of deforming free surface, liquid motions are intense and are directed toward the sidewall. Weak radially inward flows are observed only in a region very close to the sidewall. As depicted in Fig. 9, vertical velocity w in the bulk of flowfield is directed downward at moderate and small radii. At high elevations (see, e.g., the curve for $z' = 0.5$) however, because of the dominant effect of deforming free surface, the liquid between the free surface and the sidewall is squeezed upward, which generates positive values of w. Figure 10a illustrates evolving vertical profiles of u along the cut $r = 0.5$. Clearly, radial flows, in general, are very weak in the interior. The initial development and subsequent decay of the Ekman layer are discernible in Fig. 10a. The vertical profiles of w at various radial cuts are displayed in Fig. 10b. For comparison purposes, the interior solutions based on the H–G prediction are shown by broken lines. As is well known, the Wedemeyer[2] and H–G[10,11] models predict that w is linear in z in the interior. It is noted that the predictions of the inviscid Wedemeyer model are mainly applicable to the region ahead of the shear front. Needless to say, the vertically linear profiles of w are applicable only to the interior region, not in the Ekman layers.

The numerical results for run 2a and run 2b are similarly arranged in Figs. 11–14. Comparisons of the free surface deformation as well as the azimuthal velocity between the numerical results and the

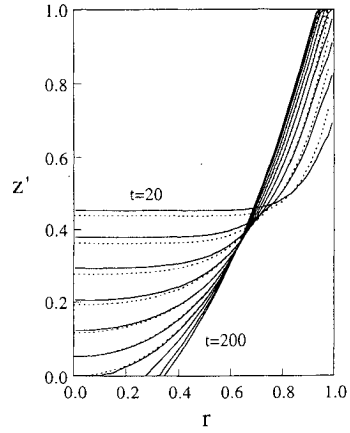

Fig. 15a Free-surface contours for run 3: ——, present results; and - - - -, predictions of H–G. Time interval for curves is $\Delta t = 20.0$.

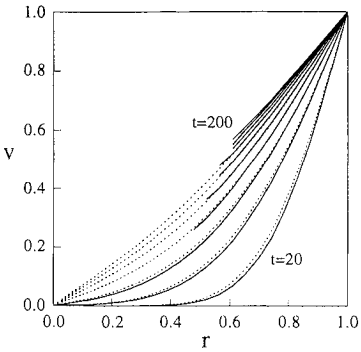

Fig. 15b Azimuthal velocity v for run 3: ——, present results; and - - - -, predictions of H–G. Time interval for curves is $\Delta t = 20.0$.

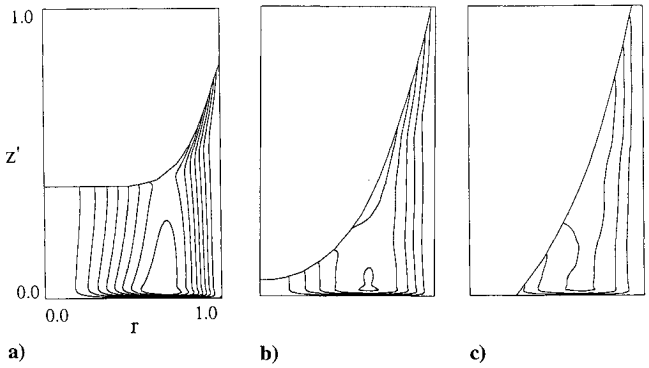

Fig. 16 Meridional streamfunction ψ for run 3: a) $t = 20.0$, $\psi_{max} = 4.50 \times 10^{-3}$, $\Delta\psi = 5.00 \times 10^{-4}$; b) $t = 60.0$, $\psi_{max} = 1.65 \times 10^{-3}$, $\Delta\psi = 3.30 \times 10^{-4}$; and c) $t = 140.0$, $\psi_{max} = 7.85 \times 10^{-4}$, $\Delta\psi = 2.62 \times 10^{-4}$.

predictions of H–G model are satisfactory, as evidenced in Figs. 11 and 13. Furthermore, the meridional flows, as shown by the numerical results in Figs. 12 and 14, are consistent with the basic conceptual picture envisioned in the H–G model. The plots of meridional streamfunctions are illustrative of the role of time-dependent Ekman layer and of the meridional flows induced by the deformation of the free surface. In a similar fashion, the numerical results for run 3 are displayed in Figs. 15 and 16. These plots are demonstrative of the good agreement between the present numerical results and the predictions of the H–G model.

IV. Conclusions

Numerical solutions to the governing Navier–Stokes equations have been secured. Comprehensive results for four prototypical flow configurations are presented for detailed examination.

The shape of the evolving free surface has been captured numerically. For all of the four exemplary runs, the numerical results are in close agreement with the predictions of the H–G model. The transient azimuthal velocity field is also described, and the two sets of results are mutually consistent.

Taking advantage of the wealth of numerical data, scrutiny is made of the detailed profiles of the meridional velocity components. The initial development and subsequent weakening of the Ekman layer are captured well by the numerical solutions. The transient meridional flowfield, as constructed by the numerical solutions, is consistent with the fundamental conceptual picture incorporated in the H–G model.

The present numerical study is in support of the basic contentions as well as the prediction capabilities of the H–G model.

References

[1]Greenspan, H. P., and Howard, L. N., "On a Time Dependent Motion of a Rotating Fluid," *Journal of Fluid Mechanics*, Vol. 17, Pt. 3, 1963, pp. 385–404.

[2]Wedemeyer, E. H., "The Unsteady Flow Within a Spinning Cylinder," *Journal of Fluid Mechanics*, Vol. 20, Pt. 3, 1964, pp. 383–399.

[3]Watkins, W. B., and Hussey, R. G., "Spin-up from Rest in a Cylinder," *Physics of Fluids*, Vol. 20, Oct. 1977, pp. 1596–1604.

[4]Weidman, P. D., "On the Spin-Up and Spin-Down of a Rotating Fluid. Part 1: Extending the Wedemeyer Model. Part II: Measurements and Stability," *Journal of Fluid Mechanics*, Vol. 77, Pt. 4, 1976, pp. 685–735.

[5]Kitchens, C. W., Jr., "Navier–Stokes Solutions for Spin-Up in a Filled Cylinder," *AIAA Journal*, Vol. 18, No. 8, 1980, pp. 929–934.

[6]Hyun, J. M., "Spin-Up from Rest in a Differentially-Rotating Cylinder," *AIAA Journal*, Vol. 21, No. 9, 1983, pp. 1278–1282.

[7]Hyun, J. M., Leslie, F., Fowlis, W. W., and Warn-Varnas, A., "Numerical Solutions for Spin-Up from Rest in a Cylinder," *Journal of Fluid Mechanics*, Vol. 127, Feb. 1983, pp. 263–281.

[8]Ibrani, S., and Dwyer, H., "Flow Interactions During Axisymmetric Spin-Up," *AIAA Journal*, Vol. 25, No. 10, 1987, pp. 1305–1311.

[9]Goller, H., and Ranov, T., "Unsteady Rotating Flow in a Cylinder with a Free Surface," *Journal of Basic Engineering*, Vol. 90, No. 4, 1968, pp. 445–454.

[10]Homicz, G. F., and Gerber, N., "Numerical Model for Fluid Spin-Up from Rest in a Partially Filled Cylinder," AIAA Paper 86-1211, May 1986.

[11]Homicz, G. F., and Gerber, N., "Numerical Model for Fluid Spin-Up from Rest in a Partially Filled Cylinder," *Journal of Fluid Engineering*, Vol. 109, June 1987, pp. 194–197.

[12]Choi, S., Kim, J. W., and Hyun, J. M., "Experimental Investigation of the Flow with a Free Surface in an Impulsively Rotating Cylinder," *Journal of Fluids Engineering*, Vol. 111, Dec. 1989, pp. 439–442.

[13]Choi, S., Kim, J. W., and Hyun J. M., "Transient Free Surface Shape in an Abruptly Rotating, Partially Filled Cylinder," *Journal of Fluids Engineering*, Vol. 113, June 1991, pp. 245–249.

[14]Gerber, N., "Properties of Rigidly Rotating Liquids in Closed Partially Filled Cylinder," *Journal of Applied Mechanics*, June 1975, pp. 734, 735.

[15]Warn-Varnas, A., Fowlis, W. W., Piacsek, S., and Lee, S. M., "Numerical Solutions and Laser-Doppler Measurements of Spin-Up," *Journal of Fluid Mechanics*, Vol. 85, April 1978, pp. 609–639.

[16]Patankar, S. V., *Numerical Heat Transfer and Fluid Flow*, 1st ed., McGraw–Hill, New York, 1980, Chaps. 2–9.

[17]Hirt, C. W., and Nichols, B. D., "Volume of Fluid (VOF) Method for the Dynamics of Free Boundaries," *Journal of Computational Physics*, Vol. 39, 1981, pp. 201–225.

[18]Peyret, R., and Taylor, T. D., "Projection Method," *Computational Methods for Fluid Flow*, Springer–Verlag, New York, 1983, Chap. 6.

[19]Lim, T. G., Choi, S. M., and Hyun, J. M., "Transient Interface Shape of a Two-Layer Liquid in an Abruptly Rotating Cylinder," *Journal of Fluids Engineering*, Vol. 115, June 1993, pp. 324–329.